GARY WATSON

REFRACTION MODELING OF INTERNAL WAVES IN A TWO-LAYER SYSTEM, AS OBSERVED IN THE STRAIT OF GIBRALTAR

The theory and application for a model of the refraction of small-amplitude gravity waves on the interface between two layers of fluid are described. Each fluid is vertically uniform, but may have an arbitrary horizontal distribution of depth, density, and current. As an example, it is shown that this model predicts quite well the shapes of internal waves in the Strait of Gibraltar, which were observed using a shore-based marine radar.

INTRODUCTION

Internal gravity waves are propagating vertical oscillations within the body of a density-stratified medium such as the ocean or the atmosphere. When there is a decrease in density with height, an element of fluid that is displaced upward (or downward) is subject to a restoring force because it is denser (or lighter) than the surrounding fluid. In the ocean, internal waves can be generated by mechanisms such as atmospheric pressure fluctuations, ice motion, ships, and flow over topography. Such waves have often been observed in data from moored instruments and in remotely sensed images of the ocean surface. The latter is possible because the internal wave motion induces surface currents with horizontal gradients. These currents modulate the surface wave spectrum above the internal waves, and thus the local intensity of the image in question. In the case of radar, for example, the backscattering cross section of microwaves is dependent on the surface wave spectrum, and so the radar image exhibits intensity modulations that mark the positions of the internal waves. This

phenomenon has been the subject of much study over the past decade (see, for example, Refs. 1 and 2, and the article in this issue by Gasparovic, Thompson, and Apel.

The unique contribution of the data being modeled here was to provide a long time series of images of an area within which many internal waves were observed. This allowed their propagation and refraction to be studied in some detail. The purpose of this article is to describe a numerical model that was used to simulate the refraction of those waves. The results from the model are discussed more fully in Ref. 3.

The images were from a shore-based X-band marine radar that monitored the eastern end of the Strait of Gibraltar during March and April 1986.[3,4] Figure 1 is a chart of the Strait showing the bathymetry, the location of the radar at Gibraltar, and the approximate area that was imaged (tinted area). The main waves imaged by this radar were associated with a large internal undular bore that regularly propagates through the Strait. (An internal undular bore is a propagating net change


Figure 1. Bathymetric chart of the Strait of Gibraltar. The location of the radar is indicated, and the approximate area of coverage is shown by the light blue area. The red lines indicate the location of the internal wave features imaged in Figure 2. The blue lines are depth contours. Tidal flow over Camarinal Sill is the source of these waves.
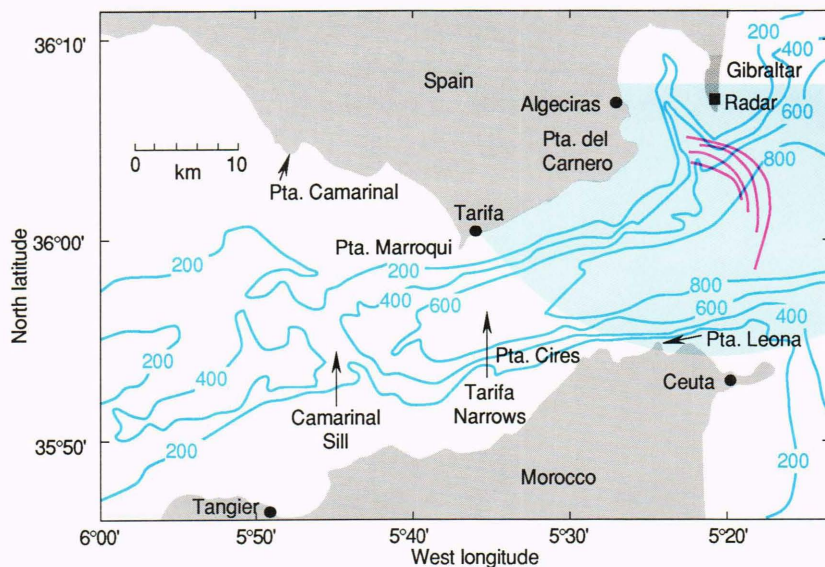
in isopycnal displacement that is accompanied by wave-like oscillations.) The internal waves are generated during the westward tidal flow over Camarinal Sill. They are released near high water and then propagate eastward along the interface between the upper layer of Atlantic water and the lower layer of Mediterranean water. This two-layer structure results from an exchange flow between the two seas, in which evaporation from the Mediterranean is replenished by an eastward flow of relatively fresh Atlantic water, and the salt balance is maintained by a slightly weaker westward flow of saltier Mediterranean water. The salinity difference provides the main source of density stratification. Because the upper layer is shallow (~ 60 m) relative to the wavelength (~ 1500 m), and the waves have large amplitudes (up to ~ 50 m peak-to-peak), the waves cause strong surface current gradients ($\sim 10^{-3}$ s^{-1}) and hence strongly modulate the surface waves and their radar backscattering cross section.

Figure 2 is an example of one of the radar images, chosen because it shows the passage of an internal wave packet during a period when the features were visible across a particularly large portion of the width of the Strait (≈ 17 km). It was taken 7 h and 40 min after high water on 14 April 1986. The location of the waves is shown by the curved lines in Figure 1; they have propagated along the length of the Strait and are emerging into the Mediterranean Sea. This image is from a sequence taken at intervals of 3 min, which reveals the waves to have a phase speed of ≈ 1.7 m/s (Fig. 3).

The question is raised as to what factors determined the shape into which these waves have been refracted. Any property that varies with position within a medium, and on which the dispersion relation is dependent, will normally cause some amount of refraction because different parts of a wave front will be moving at different speeds. The relative importance of such properties may be investigated using a numerical propagation model that simulates the effects on the wave refraction of changing the properties of the medium.
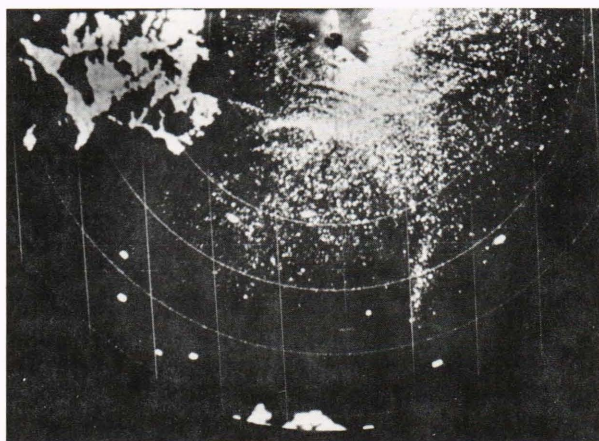

Figure 2. Part of the radar image recorded at 1207 GMT, 14 Apr 1986 (high water + 7 h 40 min). Spanish and Moroccan coasts are visible at top left and bottom center. Gibraltar is at top center, which is the center of the radar screen. Range rings are at intervals of 2 nmi (3.7 km). Several ships are present. Three or four internal waves are discernible as intensity variations in the sea surface scatter (see the curved lines in Fig. 1). The first of these is visible across a particularly high proportion of the Strait, as a result of favorable imaging conditions.

This article describes such a model, which was developed for use with the Strait of Gibraltar. The theory and implementation are described in sufficient detail for a similar model to be constructed by the reader. A sample result is given, but a more complete account of the results and conclusions, and of the data on which the model is based, may be found in Ref. 3.

REFRACTION THEORY

The medium to be modeled is horizontally nonuniform, anisotropic (because of the currents), and time-dependent (because of the tides). The waves under study are known to have large enough amplitudes to exhibit nonlinear behavior. The use of a complete theory to
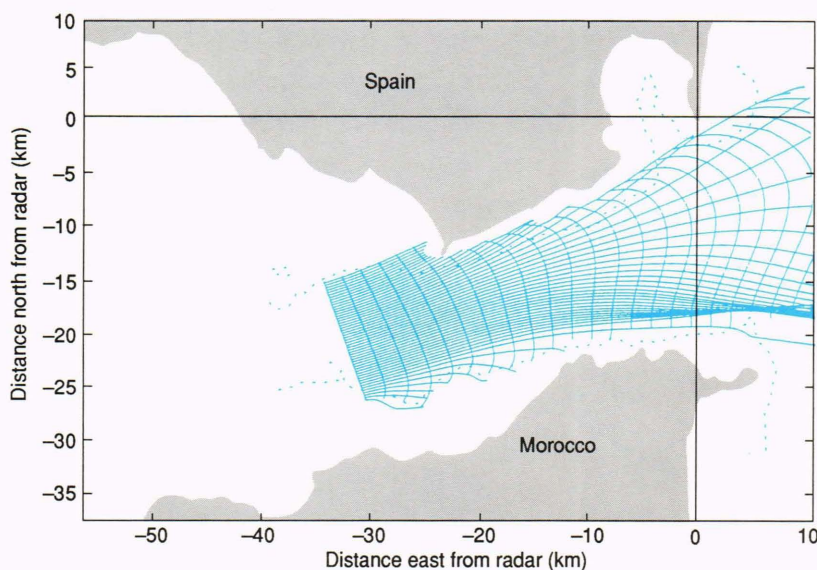
Figure 3. Result of Run 33. Dotted line is the 200-m contour. Lines running from left to right are group rays, and those running from top to bottom are wave fronts.

simulate such a system would be too demanding numerically and in any case would not be justified, because insufficient data are available to specify all of the necessary parameters. Rather, a simplified model was chosen that uses linear (i.e., restricted to waves of infinitesimal amplitude), two-layer, time-independent theory based on measurements of the time-averaged stratification and currents. In other words, the effects of large-amplitude waves, of continuously variable stratification and shear, and of tides were not included. It will be seen, however, that these are not necessary to produce modeled wave shapes similar to those observed.

The theory used is similar to the theory of ray optics, and its application is generally referred to as ray tracing. The main results are included here; more rigorous derivations may be found in Refs. 5 and 6. This theory is also used when calculating the surface wave modulation caused by the surface currents of internal waves.[7] What follows is a summary of the general, time-dependent theory that is then simplified into the time-independent theory used in the refraction model.

Two assumptions are made to simplify the situation:

1. The wave field is assumed to have been well dispersed since the initial disturbance, so that at any point only one spectral component is present; in other words, there is a well-defined local frequency and wave vector at each point in the field. In this case, the waves are "nearly plane," and the wave field may be written as

$$\psi = \Psi(\mathbf{x},t)e^{i\phi(\mathbf{x},t)} = \Psi(\mathbf{x},t)e^{i[\mathbf{k}(\mathbf{x},t)\cdot\mathbf{x}-\omega(\mathbf{x},t)t]} , \qquad (1)$$

where the amplitude, Ψ; frequency, ω; and wave vector, $\mathbf{k}$ are each functions of position and time. The local frequency of the wave field, ω, is uniquely defined at any $(\mathbf{x},t)$ by

$$\omega(\mathbf{x},t) = \omega_0[\mathbf{k}(\mathbf{x},t),\mathbf{x},t] \qquad (2)$$

(ω should be distinguished from ω_0, the dispersion relation, which is defined at all $\mathbf{k}$, $\mathbf{x}$, and t).

2. The properties of the propagation medium, defined by the dispersion relation, $\omega_0(\mathbf{k},\mathbf{x},t)$, vary little over time scales of a wave period and distance scales of a wavelength.

In addition, since the internal waves being modeled are approximately confined to the pycnocline, propagation in the vertical direction is assumed to be negligible, so that $\mathbf{x} = (x,y)$ and $\mathbf{k} = (k_x,k_y)$.

Within a wave packet, assumption 1 should be good because the waves were usually observed to have long, nearly parallel wavefronts. Thus, because only one spectral component is present, the phase is uniquely defined at each point. Assumption 2 is not really valid in the Strait of Gibraltar. While the time scale of variations in the medium (one tidal cycle) is much greater than the typical wave period of 20 min, there may be substantial

differences between the properties of the medium at two points separated by 1500 m, a typical wavelength. This variation is not so rapid as to make the theory impossible to apply, however, and it is instructive to see what predictions are obtained. Results from those areas where the medium is varying particularly rapidly, such as near the steep topography of Camarinal Sill and the coast of Morocco, should be treated with particular caution.

An equation for the conservation of wave crests follows from Equation 1, and when this is combined with the general dispersion relation (Eq. 2), the following "ray equations" result. These give the dependence on time of the three variables Ψ, $\mathbf{k}$, and ω, along the group ray trajectories,

$$\frac{d\mathbf{x}}{dt} = \mathbf{c}_g = \nabla_\mathbf{k}[\omega_0(\mathbf{k},\mathbf{x},t)] , \qquad (3)$$

where the operator $\nabla_\mathbf{k}$ is $(\partial/\partial k_x,\partial/\partial k_y,\partial/\partial k_z)$. $\mathbf{c}_g$ is the group velocity of waves with wave vector $\mathbf{k}$ in a medium with properties defined at the position $\mathbf{x}$ and time t. Along such trajectories,

$$\frac{d\mathbf{k}}{dt} = -\nabla[\omega_0(\mathbf{k},\mathbf{x},t)] , \qquad (4)$$

$$\frac{d\omega}{dt} = \frac{\partial}{\partial t}[\omega_0(\mathbf{k},\mathbf{x},t)] , \qquad (5)$$

and

$$\frac{1}{A}\frac{dA}{dt} = -\nabla\cdot[\mathbf{c}_g(\mathbf{k};\mathbf{x},t)] . \qquad (6)$$

Equation 6 represents the conservation of wave action and determines the change of wave amplitude along a ray. This equation states that there is no flux of wave action across group rays, so that A is directly related to the density of group rays. A is the wave action density, which is related to the energy density, E, by

$$A = \frac{E}{\omega} = \frac{\alpha\Psi^2}{\omega} . \qquad (7)$$

The constant of proportionality, α, depends on which wave variable is represented by Ψ; it may be dependent on the properties of the medium and hence on position.

If the medium is time-independent, the equations become

$$\omega(\mathbf{x}) = \omega_0[\mathbf{k}(\mathbf{x}),\mathbf{x}] \ (= constant) , \qquad (8)$$

$$\psi = \Psi(\mathbf{x})e^{i\phi(\mathbf{x})} = \Psi(\mathbf{x})e^{i[\mathbf{k}(\mathbf{x})\cdot\mathbf{x}-\omega(\mathbf{x})t]} , \qquad (9)$$

$$\frac{d\mathbf{x}}{dt} = \mathbf{c}_g = \nabla_\mathbf{k}[\omega_0(\mathbf{k},\mathbf{x})] = \mathbf{F}(\mathbf{k},\mathbf{x}) , \qquad say, \quad (10)$$

$$\frac{d\mathbf{k}}{dt} = -\nabla[\omega_0(\mathbf{k,x})] = \mathbf{G(k,x)} \ , \tag{11}$$

$$\frac{d\omega}{dt} = 0 \ , \tag{12}$$

and

$$\frac{1}{A}\frac{dA}{dt} = -\nabla \cdot [\mathbf{c}_g(\mathbf{k;x})] \ . \tag{13}$$

Note that the operator d/dt is evaluated along a group ray (defined by Eq. 10) in each case. Equations 10 and 11 are a pair of coupled ordinary differential equations that may be solved numerically, given values of $\mathbf{k}$ and $\mathbf{x}$ at the beginning of each group ray, because the variables $\mathbf{k}$ and $\mathbf{x}$ evolve along each ray independently from all other rays. Note two facts that greatly simplify the computations in the time-independent case:

1. The frequency ω is constant (Eq. 12).
2. $\mathbf{k}$ is a function of position only and so values of $\mathbf{k}$ calculated at any time (using Eq. 11) may be used in Equation 9 to obtain an instantaneous picture of the wave field.

Remembering that (as may be seen from Eq. 9) the wave vector $\mathbf{k}$ is defined in terms of the phase ϕ by

$$\mathbf{k} = \nabla\phi \ , \tag{14}$$

it must be that

$$\nabla \times \mathbf{k} = 0 \tag{15}$$

is always satisfied. This result may be used to test the consistency of the calculated $\mathbf{k}$ field.

NUMERICAL SOLUTION OF THE RAY EQUATIONS

Of the various integration schemes that are available for the solution of differential equations, the centered scheme, in which Equation 10 would be written

$$\frac{\mathbf{x}_{n+1} - \mathbf{x}_{n-1}}{2\Delta t} = \mathbf{F}_n \ ,$$

is often sufficient. This was used initially, but in some cases a rapidly growing oscillation between alternate time steps was found. The prediction–correction scheme was chosen as the next most simple, but more stable, scheme. Here, the integration of Equations 10 and 11 is performed in two stages at each time step. In the first, the forward scheme is used to obtain the approximate "prediction" values,

$$\mathbf{x}'_{n+1} = \mathbf{x}_n + \mathbf{F}_n\Delta t \ , \tag{16}$$

$$\mathbf{k}'_{n+1} = \mathbf{k}_n + \mathbf{G}_n\Delta t \ . \tag{17}$$

$\mathbf{F}$ and $\mathbf{G}$ are then re-evaluated at these points to obtain an estimate of their values at the next step:

$$\mathbf{F}'_{n+1} = \mathbf{F}(\mathbf{x}'_{n+1}, \mathbf{k}'_{n+1}) \ , \tag{18}$$

$$\mathbf{G}'_{n+1} = \mathbf{G}(\mathbf{x}'_{n+1}, \mathbf{k}'_{n+1}) \ . \tag{19}$$

These are then used to obtain the "correction" values,

$$\mathbf{x}_{n+1} = \mathbf{x}_n + \tfrac{1}{2}(\mathbf{F}_n + \mathbf{F}'_{n+1})\Delta t \ , \tag{20}$$

$$\mathbf{k}_{n+1} = \mathbf{k}_n + \tfrac{1}{2}(\mathbf{G}_n + \mathbf{G}'_{n+1})\Delta t \ . \tag{21}$$

Thus, each pair of $(\mathbf{k,x})$ values is calculated using the previous pair, together with values of the functions $\mathbf{F}$ and $\mathbf{G}$, which are obtained numerically from Equations 10 and 11:

$$F_x = c_{gx}$$
$$= \frac{\omega_0(k_x + \Delta k_x, k_y, x, y) - \omega_0(k_x - \Delta k_x, k_y, x, y)}{2\Delta k_x} \ , \tag{22}$$

$$F_y = c_{gy}$$
$$= \frac{\omega_0(k_x, k_y + \Delta k_y, x, y) - \omega_0(k_x, k_y - \Delta k_y, x, y)}{2\Delta k_y} \ , \tag{23}$$

$$G_x =$$
$$\frac{\omega_0(k_x, k_y, x + \Delta x, y) - \omega_0(k_x, k_y, x - \Delta x, y)}{2\Delta x} \ , \tag{24}$$

$$G_y =$$
$$\frac{\omega_0(k_x, k_y, x, y + \Delta y) - \omega_0(k_x, k_y, x, y - \Delta y)}{2\Delta y} \ . \tag{25}$$

Values of $\Delta x = \Delta y = 1.0$ m, and $\Delta k_x = \Delta k_y = 10^{-5}$ m^{-1} were used. Smaller values were found to give spurious results because of rounding errors.

The starting positions of the rays, $\mathbf{x}_{r1}$ (r is the ray number), defined the curve of the initial wavefront. The initial $\mathbf{k}$ values, $\mathbf{k}_{r1}$, were then evaluated by prescribing them to be in the direction of the axis and searching to find the correct magnitude, k, to solve Equation 8 with $\omega = 2\pi/1200$ rad/s. Using a time step of $\Delta t = 120$ s, the integration of Equations 16 through 21 was then carried out from these starting values, until a point in $\mathbf{k},\mathbf{x}$ space was reached where ω_0 could not be evaluated (usually where the interface met the bottom), or until a certain number of time steps had elapsed. It should be noted that if the frequency is not initially set to be the same everywhere, condition 15 is not satisfied, so the initial $\mathbf{k}$ field is physically incorrect.

VERIFICATION OF RESULTS

The resulting $\mathbf{k}_{rn}, \mathbf{x}_{rn}$ were used to evaluate ϕ_{rn}, by integration of Equation 14 along two different paths, from $\phi = 0$ along $n = 1$ (Fig. 4):

1. ϕ_1:

On $\overline{AB}$, $\phi_1 = 0$.

On $\overline{BD}$, $\phi_{1,r,n+1} =$

$\phi_{1,r,n} + 0.5(\mathbf{k}_{r,n+1} + \mathbf{k}_{r,n}) \cdot (\mathbf{x}_{r,n+1} - \mathbf{x}_{r,n})$.

2. ϕ_2:

On $\overline{AC}$, $\phi_{2,r,n+1} =$

$\phi_{2,r,n} + 0.5(\mathbf{k}_{r,n+1} + \mathbf{k}_{r,n}) \cdot (\mathbf{x}_{r,n+1} - \mathbf{x}_{r,n})$.

On $\overline{CD}$, $\phi_{2,r+1,n} =$

$\phi_{2,r,n} + 0.5(\mathbf{k}_{r+1,n} + \mathbf{k}_{r,n}) \cdot (\mathbf{x}_{r+1,n} - \mathbf{x}_{r,n})$.

Because $\nabla \times \mathbf{k} = 0$ (Eq. 15), the integral should be path-independent; ϕ_1 and ϕ_2 were compared in order to check the consistency of the calculated $\mathbf{k}$ field with this condition.

For runs without the inclusion of uneven bottom topography, the discrepancy between the phases, ϕ_1 and ϕ_2, was typically less than 0.1 rad. This is an insignificant fraction of a wavelength, confirming that the model was working properly and that the ray spacing and time step were fine enough.

With the inclusion of the real depth field, the discrepancy was rarely greater than ~ 2 rad within the body of the wave field. This is approximately a third of a wavelength and would have a slight effect on wave front shape. This is most likely because the approximation of a slowly varying wave field is not valid in the presence of such a rapidly changing variable (the depth changes particularly rapidly as the shores of the Strait are approached). Although it should be noted, an error of less
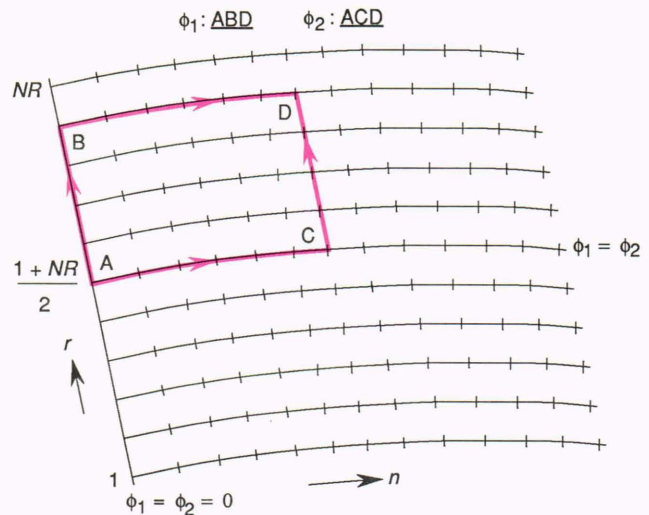

Figure 4. Integration paths used to evaluate the internal wave phase, ϕ, from the wave vector, $\mathbf{k}$. Ticks show integration steps along each group ray, and the heavy line shows the two paths: $\overline{ABD}$ for ϕ_1 and $\overline{ACD}$ for ϕ_2. r is the ray index and n the step index. $\overline{AB}$ lies on the "starting line," along which $\phi_1 = \phi_2 = 0$. $\overline{AC}$ lies along the central ray $r = (1 + NR)/2$, where NR is the number of rays) so that here, ϕ_1 and ϕ_2 are equal.

than a wavelength is not serious when it is mainly the qualitative features of the refraction that are under study.

Some large discrepancies (of order 10^2 rad) were detected in several of the runs in which all the parameters were included. They are unimportant because they were associated with a few rays that followed paths very different from those of their neighbors, such as that at the lower right in Figure 3. In this instance the function χ, which models the horizontal shear, is causing some of the rays to focus in an unrealistic manner.

PRESENTATION OF RESULTS

The positions of successive wave fronts were then calculated by finding lines of constant ϕ at intervals of 2π. A simple contouring routine was written to do this; it searched along each ray to estimate, by interpolation, the position of each required value of ϕ. ϕ_1 was actually used for ϕ, being considered more reliable than ϕ_2, because the value of the integral is known to be exactly zero along $\overline{AB}$.

The occurrence of focusing in parts of the Strait meant that care was required when joining these points to plot wave front positions. Points were joined only on adjacent rays whose trajectories had not crossed. A test was also carried out to verify that the calculated wave front was approximately perpendicular to the local direction of $\mathbf{k}$, as it should be. This was sometimes not the case in areas where adjacent rays had followed dissimilar paths and had become well separated. An angle of 15° was chosen as a threshold; if the discrepancy was larger than this, the wave front was not plotted.

In the time-independent case, the solution for $\mathbf{k}$ may be taken as representing a continuous, monochromatic train of waves being fed into the Strait along the start-

ing line. The lines of constant phase are also the successive positions of any one wave front at time intervals of the wave period, $2\pi/\omega$. They may thus be directly compared with successive positions of wave fronts observed using the radar, despite the fact that the real waves occur in groups. It would be possible to simulate group behavior by using a time-dependent model and modulating the initial wave amplitude.

Although Equation 13 was not solved, qualitative information about the distribution of wave energy may be obtained from the distribution of group rays. Energy is concentrated where they are focused and diluted where they are dispersed.

The group rays and wave fronts were plotted as the final output of the model. These are the most useful quantities; group rays indicate the distribution of wave energy, and it is wave fronts that were observed by the radar and so are directly comparable with the images. The plot in Figure 3 shows only alternate group rays in order to make them less dense. The coastline and the 200-m contour are also shown.

APPLICATION TO THE STRAIT OF GIBRALTAR

The model outlined above may be applied to any physical system whose dispersion relation, $\omega_0(\mathbf{k},\mathbf{x})$, is known. For internal waves in a shear flow, the full linear dispersion relation is obtained by solving a differential equation for the eigenfunction (which specifies how the wave amplitude varies with depth), given the boundary conditions of zero amplitude at the surface and the bottom. The equation is known as the Taylor–Goldstein equation.[3] To use the equation, however, requires a detailed knowledge of the stratification and shear at each location in the Strait—information that is not available. The Strait was instead modeled as a two-layer system,

the dispersion relation of which is known analytically (for infinitesimal waves):

$$
\omega_0 = \Big((\rho_1 c_1 \mathbf{U}_1 + \rho_2 c_2 \mathbf{U}_2)\cdot\mathbf{k} + \{gk\Delta\rho(\rho_1 c_1 \\
+ \rho_2 c_2) - \rho_1\rho_2[(\mathbf{U}_2 - \mathbf{U}_1)\cdot\mathbf{k}]^2\}^{1/2} \Big) \\
\div (\rho_1 c_1 + \rho_2 c_2) . \qquad (26)
$$

Subscripts 1 and 2 refer to the upper and lower layers, respectively; ρ_i is layer density; $\Delta\rho = \rho_2 - \rho_1$; $c_i = \coth kH_i$; H_i is layer depth; $\mathbf{U}_i$ is layer current; and g is the acceleration due to gravity. This approach enables the gross features of horizontal variations in the Strait to be modeled in terms of a small number of parameters.

The dependence of the dispersion relation on $\mathbf{x}$ is through the variation in the parameters ρ_1, ρ_2, H_1, H_2, $\mathbf{U}_1$, and $\mathbf{U}_2$. Reference 3 describes how tidally averaged values of these parameters were estimated from data collected as part of the "Gibraltar Experiment,"[8] especially those of Armi and Farmer.[9,10] The results are summarized below and shown schematically in Figure 5.

No evidence was found of any systematic variation of the layer densities ρ_1 and ρ_2 within the Strait. The values $\rho_1 = 1027.06$ and $\rho_2 = 1028.99$ kg/m^3 were used throughout, based on the mean of several conductivity–temperature–depth (CTD) profiles in the central Strait.

Rather than H_1 and H_2, the parameters used to specify the layer depths were H_1 and the total depth $H = H_1 + H_2$. H was obtained from a survey chart using a 1-km grid, and a bicubic spline was then fitted to the data so that H was continuous everywhere. To clar-

Figure 5. Illustration of parameters used in the model; H_1 = upper layer depth, H_2 = lower layer depth, $\mathbf{U}_1$ = upper layer current, $\mathbf{U}_2$ = lower layer current, d_1 = distance along Strait, d_2 = distance across Strait, $\chi(d_1,d_2)$ = dimensionless function containing horizontal variations of current.
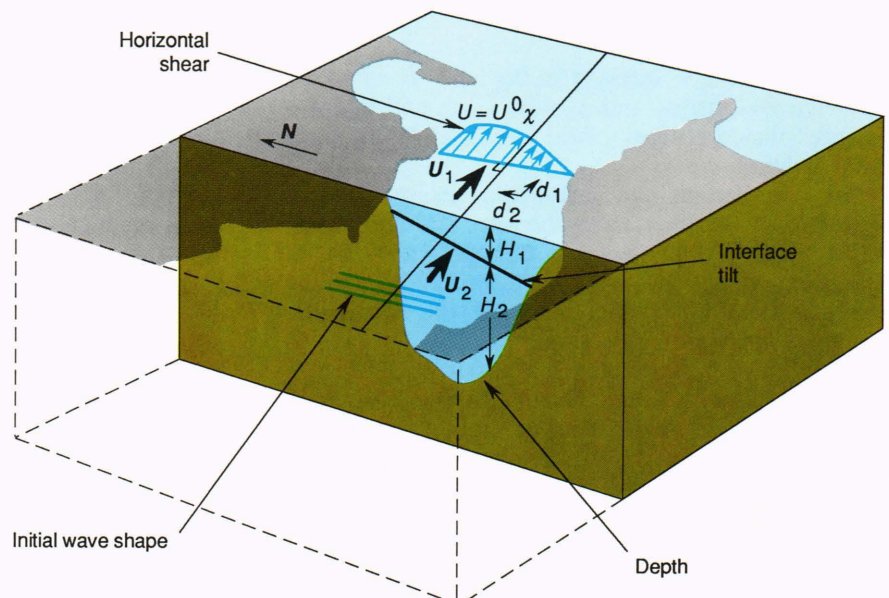
ify the model output, the coastline and 200-m contour were plotted by contouring these depth data at $H = 0$ and $H = 200$ m.

Currents in the Strait are dominated by an exchange flow that maintains the balance of both water and salt in the Mediterranean. The upper layer of Atlantic water flows eastward, and the lower layer of Mediterranean water flows westward. The effect of the Coriolis force on this exchange flow is to induce a cross-Strait slope on the interface, so that H_1 is 50 to 100 m greater at the southern boundary of the Strait than at the northern boundary. This can be thought of as the Coriolis force pushing the upper layer southward and the lower layer northward, tilting the interface so that it is deeper in the south and more shallow in the north. The resulting long-term flow is in approximate geostrophic balance. Data from several cross-Strait CTD and expendable bathythermograph (XBT) transects allowed a mean cross-Strait gradient of $\gamma = 5.5 \times 10^{-3}$ to be deduced. Because internal wave phase speed is strongly dependent on interface depth, this interface tilt will refract the waves, steering rays to the north and tending to align wavefronts east–west.

Based on data from along-Strait transects, a mean value of $H_1 = 65$ m was deduced for the upper layer depth on the central axis of the Strait. Thus, in terms of the distance d_2 from the axis (Fig. 6),

$$H_1 = 65 - \gamma d_2 \ .$$

The lower layer depth was always set to $H_2 = H - H_1$. Whenever H_1 or H_2 became zero or less, integration along the ray was terminated.

$\mathbf{U}_1$ and $\mathbf{U}_2$ were always kept along the axis of the Strait:

$$\mathbf{U}_1 = U_1 \begin{pmatrix} \cos 17° \\ \sin 17° \end{pmatrix} ,$$

$$\mathbf{U}_2 = U_2 \begin{pmatrix} \cos 17° \\ \sin 17° \end{pmatrix} .$$

U_1 and U_2 on the axis of the Strait were chosen so that the dispersion relation resulting from Equation 26 would fit as accurately as possible the dispersion relation obtained from solution of the Taylor–Goldstein equation using measurements of the time-averaged stratification and shear, $\rho(z)$ and $U(z)$, respectively.[3] With H_1 at the pycnocline and mean values ρ_1 and ρ_2 of the density in each layer, this required the values $U_1 = U_2 = 0.72$ m/s. This was somewhat unexpected, since it corresponds to the absence of shear between the two layers—a uniform current, independent of depth. Several factors may contribute to this result. First, the two-layer model is not a particularly good way of representing the effects of vertical shear, because it has an infinite current

gradient at the interface. Second, available data suggest that the shear region lies somewhat below the density interface, so that the upper layer current has the dominant effect on wave propagation. The value of 0.72 m/s is consistent with measurements of the mean current at the depth of the interface.

Horizontal variations in U_1 and U_2 were based on several cross-Strait transects using profiling acoustic current meters. They showed the strength of the flow gradually increasing to a maximum north of the Strait axis, with the shear being at its greatest near the narrowest part of the Strait. A dimensionless scaling function, χ, was used to simulate the along- and cross-Strait variation of current. The base values of $U_1^0 = U_2^0 = 0.72$ m/s were used, and the local values of U_1 and U_2 were found from

$$U_i = U_i^0 \chi(d_1, d_2) \ , \tag{27}$$

where d_1 and d_2 are distances along and across the Strait, respectively (Fig. 6). Figure 6 also shows the x,y coordinate system used in Equations 16 through 25.

The functions that were used in the various runs are crude representations of the observations that there was a greater current to the north and that the horizontal shear was greatest in the central part of the Strait.

In addition, two other factors will affect the shape into which the waves are refracted. The initial shape of the wave fronts may well be asymmetric, because of the complex topography of the sill region where the waves are generated. For simplicity, a straight line was used from which to start the rays. The initial position of the starting line over the crest of the sill was abandoned because it was found that the rapidly varying topography there caused very strong refraction. Many of the rays underwent strong focusing or divergence, so that no useful wave fronts were obtained in the eastern Strait. A new line was chosen 3 km east of the sill; the problem did not recur there, and this line was used for the remainder of the experiments. The line was oriented perpendicular to the chosen Strait axis (073°T).

Further, because the dispersion relation is frequency-dependent, the shape into which waves are refracted is expected to depend on the wave frequency. A wave period of 1200 s was chosen for most of the runs, being typical of the waves in the Strait.

SAMPLE RESULT

Figure 3 shows the result of Run 33, which was found to give the best agreement with measurements from the radar image sequence from which Figure 2 was taken (for a comparison, see Fig. 7). In this run, the bottom depth and interface slope were included as described above. No modification to them was necessary, suggesting that the model simulates their effects well, as far as these data are able to test.

Several different forms of the function χ were tried, each of which was broadly consistent with the current
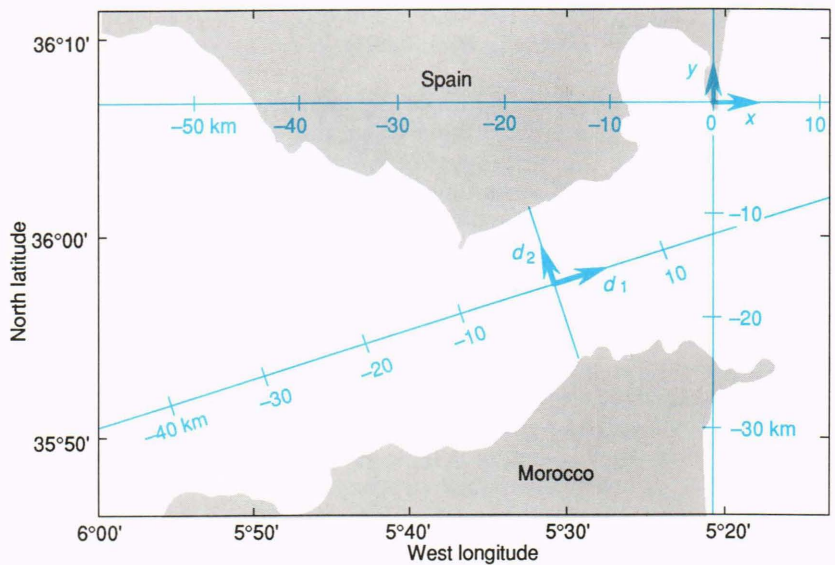
Figure 6. Coordinate systems; x,y was used for the position vector **x** in the ray tracing; d_1,d_2 (oriented along the axis of the Strait) was used when defining the cross-Strait variation of the parameters H_1, H_2, U_1, and U_2.

data mentioned above. The resulting refraction pattern was somewhat dependent on the form of χ. That which agreed best with Figure 2 was as follows and was used to give the result in Figure 3 (values of d_i are in kilometers):

$$d_1 < 0 \begin{cases} d_2 > 5.7 & \chi = 1 + 0.5\delta \\ -5.7 < d_2 < 5.7 & \chi = 1 + 0.5\delta \sin \dfrac{d_2}{5.7} \dfrac{\pi}{2} \\ d_2 < -5.7 & \chi = 1 - 0.5\delta \end{cases}$$

$$d_1 > 0 \begin{cases} d_2 > 5.7 & \chi = 1.5 \\ -5.7 < d_2 < 5.7 & \chi = 1 + 0.5 \sin \dfrac{d_2}{5.7} \dfrac{\pi}{2} \\ d_2 < -5.7 & \chi = 0.5 \end{cases},$$

where

$$\delta(d_1) = e^{-(d_1/11.4)^2} .$$

Although many wave fronts were observed during the experiment, it is not easy to define a "mean shape" of them all, with which to compare the model predictions. Except for the observation that some wave fronts had "corners" in them, possibly resulting from strong refraction where they pass through a front at the northern edge of the inflowing Atlantic water, no major differences were observed in the shapes of the wave fronts. Figure 2 was chosen as representative because this wave packet was observed out to a noticeably greater range than any of the others.

A plot of the progress of the rear of the longest wave front (as measured at 15-min intervals from the sequence of radar images of which Fig. 2 forms a part) is given in the lower part of Figure 7. The predicted wave fronts
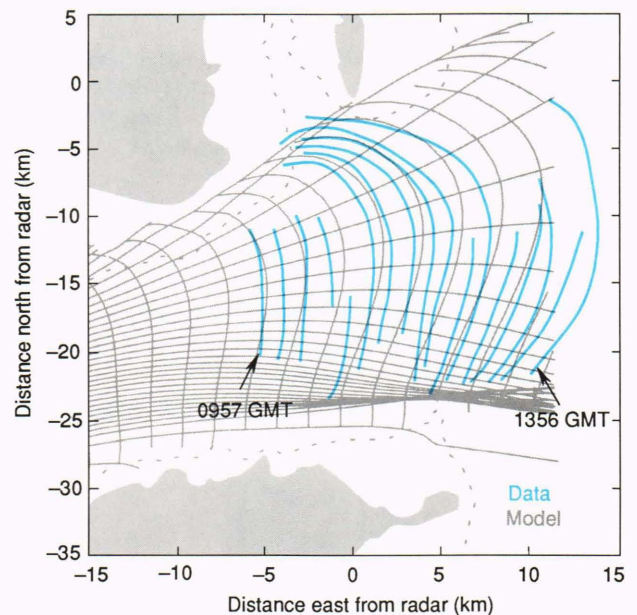
Figure 7. Comparison of modeled and observed wave front shapes: Run 33 and wave packet 17a. Gray lines are taken from Figure 3. The blue lines show positions of rear of long wave front in Figure 2, measured from sequence of radar images at 15-min intervals. The model represents an instantaneous picture of the wave field, so that the distance between wave fronts is not directly comparable between plots. The shape of the wave fronts is comparable because the model is time-independent (see text).

from Figure 3 are plotted in the upper part. The comparison is quite good, considering the number of approximations that were made in the model, although it must be admitted that the horizontal shear was adjusted to give the best fit. The greatest angle between the measured and observed wave fronts is $\sim 20°$. This figure demonstrates that the simple model incorporates all of the most important factors contributing to the wave front

shape. These results suggest that further improvements (for example, the inclusion of time-dependence and non-linearity) are unlikely to introduce any qualitative differences; it would be interesting to see whether this is the case.

It is also interesting to note that several papers have reported a larger wave amplitude in the south of the Strait than in the north.[11,12] From the density of group rays in Figure 3, it is evident that the model exhibits a concentration of internal wave energy into the south of the Strait. This was observed only when horizontal current shear was included, suggesting that this shear causes the concentration of wave energy into the southern Strait.

CONCLUSIONS

The model as outlined above has been found to work reliably, giving stable solutions with a variety of parameters representing the Strait. Fewer than 35 runs were required to produce wave front shapes that looked like those observed in the data. It demonstrated that each of the physical parameters has some effect on the shape of waves as they pass Gibraltar. The interface tilt and horizontal shear were found to be primary effects, whereas the effect of water depth was important only near the sides of the Strait. Each of these factors should be taken into account to reproduce the wave front shapes as observed near Gibraltar.

The linear, time-independent model, using simple approximations to the observed properties of the Strait, predicted wave fronts shaped similarly to those observed, suggesting that the tides do not greatly affect the gradients of properties across the Strait. It is known, however, that the phase of the tidal currents varies by several hours across the Strait; this would introduce time-dependence into the horizontal shear. A time-dependent model would be necessary to assess whether this effect is large enough to change the wave shape. This might not be worthwhile until better data are available on the horizontal dependence of tidal currents in the Strait.
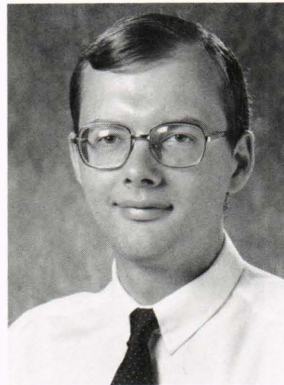
A further improvement to the model would be the determination of wave action density using Equation 6 to make quantitative predictions of wave amplitude. Finally, a nonlinear model could be attempted. The appropriate theory for nonlinear ray tracing is available, although it is not so well developed as for linear ray tracing.

REFERENCES

[1] Hughes, B. A., and Dawson, T. W., "Joint Canada–U.S. Ocean Wave Investigation Project: An Overview of the Georgia Strait Experiment," *J. Geophys. Res.* **93C**, 12,219–12,234 (1988).
[2] Gasparovic, R. F., Apel, J. R., and Kasischke, E. S., "An Overview of the SAR Internal Wave Signature Experiment," *J. Geophys. Res.* **93C**, 12,304–12,316 (1988).
[3] Watson, G., *Internal Waves in the Strait of Gibraltar: A Study Using Radar Imagery*, Ph.D. Thesis, University of Southampton, 163 pp. (1989).
[4] Watson, G., and Robinson, I. S., "A Study of Internal Waves in the Strait of Gibraltar Using Shore-Based Marine Radar Images," *J. Phys. Oceanogr.* (in press) (1990).
[5] LeBlond, P. H., and Mysak, L. A., *Waves in the Ocean,* Elsevier, Amsterdam (1978).
[6] Lighthill, J., *Waves in Fluids,* Cambridge University Press (1978).
[7] Thompson, D. R., "Intensity Modulations in Synthetic Aperture Radar Images of Ocean Surface Currents and the Wave/Current Interaction Process," *Johns Hopkins APL Tech. Dig.* **6**, 346–353 (1985).
[8] Kinder, T. H., and Bryden, H. L., "The 1985–1986 Gibraltar Experiment: Data Collection and Preliminary Results," *Eos Trans. AGU* **68**, 786–795 (1987).
[9] Armi, L., and Farmer, D. M., "The Flow of Mediterranean Water through the Strait of Gibraltar," *Prog. Oceanogr.* **21**, 1–106 (1988).
[10] Farmer, D. M., and Armi, L., "The Flow of Atlantic Water through the Strait of Gibraltar," *Prog. Oceanogr.* **21**, 1–106 (1988).
[11] Lacombe, H., and Richez, C., "The Regime of the Strait of Gibraltar," in *Hydrodynamics of Semi-Enclosed Seas*, J. C. J. Nihoul, ed., Elsevier, New York, pp. 13–73 (1982).
[12] Gascard, J. C., and Richez, C., "Water Masses and Circulation in the Western Alboran Sea and in the Strait of Gibraltar," *Prog. Oceanogr.* **15**, 157 (1985).

THE AUTHOR

GARY WATSON was born in Bournemouth, England, in 1964 and grew up in the village of Yatton, near Bristol. He read physics at St. John's College, Oxford, obtaining the degree of B.A. in 1985. He was then a research student at the University of Southampton, a Ph.D. in physical oceanography being conferred in 1989. He is presently a Postdoctoral Research Associate at APL's Milton S. Eisenhower Research Center, investigating ship-generated internal waves and their detection using radar.